RSC Advances

PAPER

View Article Online
View Journal | View Issue

Cite this: *RSC Adv.*, 2014, **4**, 56970

Mechanical bending properties of sodium titanate ($Na_2Ti_3O_7$) nanowires†

Arixin Bo,[a] Haifei Zhan,[ab] John Bell,[a] Huaiyong Zhu[a] and Yuantong Gu*[a]

Received 3rd October 2014
Accepted 24th October 2014

DOI: 10.1039/c4ra11753k

www.rsc.org/advances

We report on the mechanical properties of sodium titanate nanowires ($Na_2Ti_3O_7$ NW) through a combination of bending experiments and theoretical analysis. $Na_2Ti_3O_7$ NWs with lateral dimensions ranging from 20–700 nm were synthesized by a hydrothermal approach. A focused ion beam (FIB) was used to manipulate the selected $Na_2Ti_3O_7$ NW over a hole drilled in an indium tin oxide substrate. After welding the nanowire, a series of bending tests was performed. It was observed that the $Na_2Ti_3O_7$ NW exhibits a brittle behavior, and a nonlinear elastic deformation was observed before failure. By using the modified Euler–Bernoulli beam theory, such nonlinear elastic deformation is found to originate from a combination of surface effects and axial elongation (arising from the bending deformation). The effective Young's modulus of the $Na_2Ti_3O_7$ NW was found to be independent of the wire length, and ranges from 21.4 GPa to 45.5 GPa, with an average value of 33 ± 7 GPa. The yield strength of the $Na_2Ti_3O_7$ NW is measured at 2.7 ± 0.7 GPa.

1. Introduction

Titanates are widely acknowledged as functional ceramic materials with attractive properties such as dielectric, piezoelectric and ferroelectric properties.[1–4] They have been broadly used as structural reinforcements in polymers, metals, and ceramic composites.[5,6] In the family of titanates, sodium titanates are emerging as materials of great interest for their novel applications in batteries,[7,8] industrial liquid waste treatment,[9] fuel-cell electrolyte[10] and catalyst.[11] In the field of Li batteries, Na-based technologies have drawn increasing attention due to the superior availability and potentially lower cost of the raw materials. In this regard, the sodium titanate has been shown to be a suitable material with favourable capacities.[8] By changing the synthetic method, various external morphologies of sodium titanate can be obtained, including nanowires (NWs) and nanotubes[9,12,13] and their internal structure can also be diversely altered.[14,15] These features have made sodium titanate a strong candidate in a broad range of applications as functional material or as substrate.[13,16–19] Nevertheless, to the best of our knowledge, the mechanical properties of $Na_2Ti_3O_7$ material have not yet been revealed.

Many studies have shown that tremendous benefits are brought to the performance of the devices by incorporating wire-like (high length to width ratio) nanomaterial structures. Taking NW batteries as an example, the major advantage of NWs, compared to their bulk counterparts, are their capability to overcome the well-known pulverization problem which is detrimental to the battery cycle life.[20] NW adsorbents are also shown to be much easier to settle compared to bulk ion exchangers so that they can be efficiently recovered from the contaminant solutions.[9] A NW-based pressure sensor has been reported to have greatly improved sensitivity and stability,[21] compared to a similar pressure sensor fabricated from bulk materials. It is clear that the rapid development of NW materials has boosted the activities in nanotechnology and nanomechanics, to the extent that understanding of the mechanical properties of NWs has become extremely important. This is because understanding nanowire mechanical properties is essential for fabrication of devices such as nanocomposite strengtheners, nanoscale interconnectors and the active components in nanoelectromechanical system (NEMS) devices.[22–24] For instance, when a NW is built into a bendable electronics,[25] whether the NW is strong enough to sustain the required bending deformation is critically important.

To date, many experimental, numerical and theoretical studies have been carried out to assess the mechanical properties of different NWs. Depending on the properties of interest, researchers have performed *in situ* tension, bending and resonance tests on NWs, though nano-scale experiments are likely to encounter intrinsic complexities (*e.g.*, manipulation and measurement uncertainties).[22,26–30] Bending experiments, typically carried out using an atomic force microscope (AFM), have

[a]*School of Chemistry, Physics and Mechanical Engineering, Queensland University of Technology, GPO Box 2434, 4001, Brisbane, QLD, Australia. E-mail: yuantong.gu@qut.edu.au; Fax: +61-7-31381469; Tel: +61-7-31381009*

[b]*Department of Material Science and NanoEngineering, Rice University, Houston, TX 77005, USA*

† Electronic supplementary information (ESI) available: ESI is available for the experimental set-up and related theoretical backgrounds. See DOI: 10.1039/c4ra11753k

been studied widely in low dimensional nanomaterials (such as nanowires and graphene) due to the relatively high spatial resolution and force measurement.[26,31–38] On the other hand, a wide range of numerical simulation schemes have been established to examine the mechanical performance of NWs under a variety of loading scenarios, *e.g.*, tension, compression, bending, vibration, and torsion.[34,39–42] However, numerical studies are usually carried out by atomistic simulations, which are relied heavily on the empirical potentials that are established from first principle calculations. Theoretically, researchers have employed continuum mechanics to interpret the mechanical properties of NWs by considering the influence of surface effects.

Though above approaches have been widely employed to examine the mechanical properties of NWs, which however are usually focused on metallic or semiconducting NWs, such as Ag, Au, or Si NWs. For the novel NWs, such as the sodium titanate ($Na_2Ti_3O_7$) NW with a layered structure, an understanding of their mechanical properties is still lacking. In the present work, we have conducted an extensive experimental investigation on the bending properties of $Na_2Ti_3O_7$ NWs. Sodium titanate NWs are synthesized *via* hydrothermal method and characterized by various methods. Then, the mechanical bending properties of individual $Na_2Ti_3O_7$ NWs are extracted experimentally through Scanning Electron Microscopy (SEM) and AFM based techniques. The bending behaviours of the NW are analyzed by utilizing modified beam theories. The Young's modulus for the $Na_2Ti_3O_7$ NWs is found to vary from 21.4 GPa to 45.5 GPa, with an average value of 33 $\pm$ 7 GPa and its yield strength is measured between 2.00 and 3.64 GPa.

2. Experimental section

In the synthesis procedure, NaOH pellets and HNO_3 (AR grade) purchased from Sigma Aldrich, and $TiOSO_4 \cdot xH_2O$ (98%) from Fluka were used. Sodium titanate nanowires ($Na_2Ti_3O_7$ NW) in this study were prepared *via* a hydrothermal reaction between a concentrated NaOH solution and an inorganic titanium salt. Specifically, 10.7 g of $TiOSO_4 \cdot H_2O$ was dissolved into 80 mL of water and stirred until the solution became clear. The resultant $TiOSO_4$ solution was mixed with a 100 mL of a 15 M NaOH solution under stirring. The white suspension was then equally divided into three 125 ml Teflon-lined stainless steel autoclaves and kept at 200 °C for 48 h to yield titanate precipitates. The white precipitate in the autoclaved mixture was recovered by centrifugation and washed with deionized water four times. Finally, the collected white powder was dried at 353 K for 24 h.

The samples were characterized by powder X-ray diffraction (XRD) and transmission electron microscopy (TEM). XRD patterns of the sample powder were recorded on a Philips PANalytical X'pert pro diffract meter equipped with graphite monochromator. Cu Kα radiation and a fixed power source (40 kV and 40 mA) were used. The XRD data were collected over a 2θ range between 3.5° and 75°, at a scanning rate of 2.5° min^{-1}. The TEM study on the samples and the HRTEM investigations were carried out on a FEI Tecnai F20 operating at 200 kV. For TEM sample preparation, the specimens were dispersed in ethanol by sonification and deposited onto a copper microgrid coated with holey carbon film. The SEM imaging was carried on Zeiss scanning electron microscopy.

$Na_2Ti_3O_7$ NWs are bridged over a trench using scanning electron microscopy (SEM) built with focused ion beam (FIB) and nanomanipulator. Prior to the welding, holes with 500–700 nm depth and length ranging from 4.5–12.5 μm trench are drilled on the ITO (indium tin oxide) glass support. Then, the selected nanowire (NW) is picked up by welding its one end to the nanomanipulator tip and placed across the trench. To mount both ends of the suspended $Na_2Ti_3O_7$ NW, the electron beam induced deposition (EBID) is used to deposit a layer of platinum to cover the $Na_2Ti_3O_7$ NW and the substrate around it.[28,49]

The measurements of the mechanical property of the $Na_2Ti_3O_7$ NW are conducted by the Nanosurf FlexAFM. The sensitivity of the AFM is calibrated by measuring a force curve on a hard ITO substrate. The selected $Na_2Ti_3O_7$ NW is located *via* a 40× optical lens on the ITO surface. Once the prepared NW is located, an AFM tip with a radius of 15 nm and a height of 10–15 μm was applied to obtain the topography profile of the fixed individual NW. The cantilever used in the test was ACLA probes (purchased from Applied NanoStructure, Inc.) are silicon probes with aluminium coating on the reflex side (Fig. S4†). Each AFM tip used was calibrated carefully using a Sader's method.[53] After obtaining the sample topography, the AFM tip was then moved precisely to the mid-point of the NW. The sample was brought to contact with the tip by piezoelectric actuator, resulting in the deflection of the cantilever and bending of the NW.

3. Results and discussion

3.1. Synthesisation and characterization

Hydrothermally synthesized $Na_2Ti_3O_7$ NWs exhibit a layered structure. The powder XRD spectrum of the product reveals its overall crystalline structure (Fig. 1a) which is in good alignment with that of $Na_2Ti_3O_7$ (PDF no. 00-059-0666), also known as sodium metatitanate. The crystal structure of $Na_2Ti_3O_7$ NW is illustrated in Fig. 1b. In these NWs, three independent Ti atoms each have six oxygen atoms in the nearest environment and the polyhedral structure formed around the Ti atoms can be viewed as strongly distorted octahedral structure. Three crystallographically independent edge-sharing octahedra are the basic building blocks for this structure. Furthermore, these blocks form a ribbon-like structure and the extension of the ribbon in the structure can be considered as a section of closely-packed layers. The free oxygen vertices of the octahedra located at the edges of the ribbons are shared by the adjacent ribbons, exhibiting a zigzag structure and within these negatively charged zigzag layers, exchangeable sodium cations can be found.[43–46]

The different dimensions of the synthesized $Na_2Ti_3O_7$ NW can be seen from a typical low-magnification TEM image (Fig. 2a). The width of the NW ranges from 20–700 nm and the

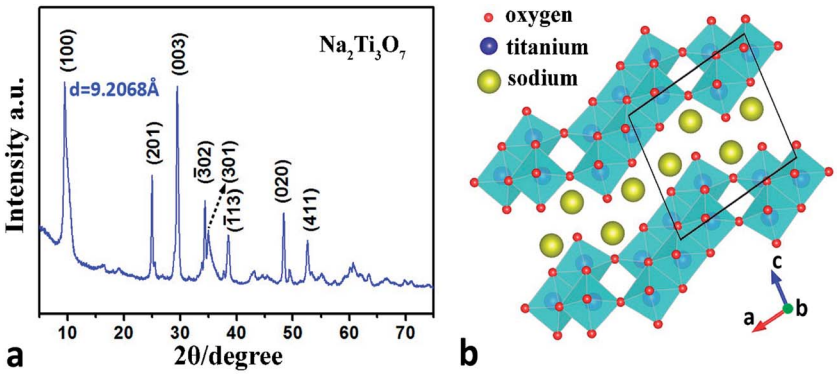

Fig. 1 (a) XRD spectrum of the synthesized $Na_2Ti_3O_7$ NW. (b) The crystal structure of sodium titanate; the black framed area shows the unit cell of the structure.

longest NW observed is around 40 μm. According to the SEM imaging and AFM topography measurement, the cross-sections of these NWs have a rectangular shape with the height-to-width ratio between 0.73–0.86. $Na_2Ti_3O_7$ NWs with various wire dimensions are pictured in the transmission electron microscopy (TEM) image and a typical cross-section area is shown in the SEM image as an inset. It should be noted that in all experiments the loading force is applied along the width direction as indicated by the arrow in the inset of Fig. 2a. An HRTEM image of a well crystallized $Na_2Ti_3O_7$ NW is taken along its [001] direction (along the nanowire) as shown in Fig. 2b. The corresponding electron diffraction pattern (Fig. 2c) indicates that the sample has a highly crystalline structure, which is in good agreement with XRD diffraction pattern. The electron diffraction pattern can be attributed to monoclinic $Na_2Ti_3O_7$ structure ($C2/m$ space group, $a = 0.808$ nm, $b = 0.378$ nm, $c = 0.916$ nm, $\beta = 94.0°$).[46]

3.2. Bending behaviours

Loading-unloading cycles were performed to investigate the bending behaviours of a single $Na_2Ti_3O_7$ NW. Prior to the bending test, a circular hole (500–700 nm deep) was drilled using focus ion beam (FIB) on ITO substrate where $Na_2Ti_3O_7$ NWs are also sparsely dispersed (Fig. S1a in ESI†). Then, a selected $Na_2Ti_3O_7$ NW is picked up using a nanomanipulator tip (Fig. S1b†) and placed across the hole. The sample preparation is completed by welding the two ends of the bridged $Na_2Ti_3O_7$ NW using electron beam induced Pt deposition (Fig. S1c†). Under AFM contact mode scanning, the topography of a bridged $Na_2Ti_3O_7$ NW is obtained before it is subjected to a force exerted at the center of the sample (Fig. S1d†). As shown in Fig. 3a, the force *vs.* displacement (F–d) curves are generally symmetric during loading and unloading processes for all three loading-unloading cycles. Such a symmetric characteristic indicates the full recovery from the deformation, signifying an elastic deformation process. Specifically, it shows that the F–d curve exhibits a linear behavior when the displacement is relatively small (curve I). When the displacement exceeds around one third of the NW height, a nonlinear deformation is observed (curve II), and the nonlinearity becomes more significant with the continuing displacement (curve III). Similar bending behavior is also observed on $Na_2Ti_3O_7$ NWs with different dimensions (Fig. S2†). According to the SEM images in Fig. 3b, the $Na_2Ti_3O_7$ NW shows no residual deformation or indent mark after unloading, which indicates that the $Na_2Ti_3O_7$ NW exhibits excellent elasticity and nonlinear elastic deformation behavior.

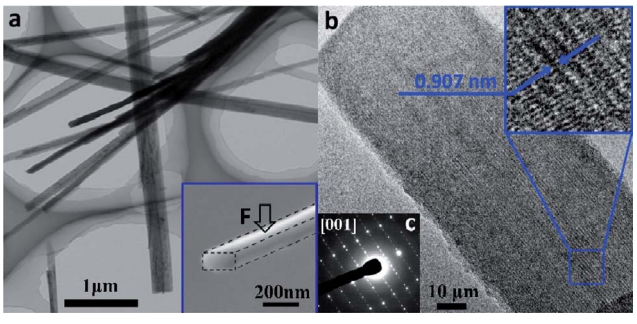

Fig. 2 (a) Low magnification TEM image of $Na_2Ti_3O_7$ NWs showing various wire dimensions; the inset is a SEM image showing the typical cross section of a NW. (b) HRTEM image of NW with a viewed down [001] with the corresponding electron diffraction patterns as shown in figure c.

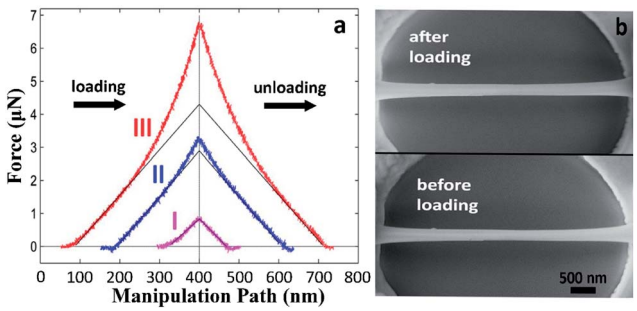

Fig. 3 (a) The F–d curves from three loading-unloading cycles recorded during manipulation. The $Na_2Ti_3O_7$ NW has a width × height of ~298 nm × 256 nm and a length of 7.5 μm. (b) SEM image showing the image of NW after and before loading under elastic deformation.

During the loading and unloading processes, an adhesive phenomenon[47] typical on AFM measurements is observed. Fig. 4a shows the AFM detection of the adhesive phenomenon where an attractive force (negative force) of ~30 nN and ~50 nN are detected during loading and unloading processes, respectively. Such attractive force originates from van der Waals force between the AFM tip and NW surface.[48] Interestingly, we found that the attractive force during unloading is generally 15–50% larger than that during loading. This can be understood while considering that the contact surface is larger during unloading, attributed mainly from the indentation induced concave NW surface (see Fig. S3†). Alternatively more surface atoms are involved in the interaction between the AFM tip and the NW surface during unloading and therefore generate stronger attractive force.

3.3. Modified beam theories

As shown in Fig. 4b, when the AFM tip approaches and starts contacting the sample surface, the force on the tip becomes repulsive and increases linearly at first for about 100 nm sample deflection. As the sample displacement increases, the measured force increases continually and nonlinearly, which eventually shift to a sudden drop from ~8 μN to ~2 μN at a displacement of 341 nm (Fig. 4b). The overall profile of the *F–d* curve is quite similar to that observed during *in situ* bending of Si NW.[49] Considering the symmetric *F–d* curves during loading-unloading cycles (Fig. 3a) and the sudden force drop, it can be concluded that $Na_2Ti_3O_7$ NW behaves like a typical brittle material. After failure, the $Na_2Ti_3O_7$ NW is fractured at the center of the bridged beam where the force is applied as shown in the SEM image of Fig. 4b inset. Extensive bending tests were carried out and the same results are shown that the $Na_2Ti_3O_7$ NW is exhibiting a nonlinear elastic deformation and brittle behavior.

The nonlinear elastic behavior of the NW can be described by the Euler–Bernoulli beam theory (EBT) model modified with the axial extension, the impact from which is normally unnoticeable at macro-scale on the bending deformation while it is profound for NWs. The governing equation is given as below:

$$(EI)\frac{d^4w}{dx^4} - T\frac{d^2w}{dx^2} = 0,\ T = \frac{(EA)}{L}\int_0^{L/2}\left(\frac{dw}{dx}\right)^2 dx \quad (1)$$

here, E is Young's modulus, w is the beam deflection. The moment of inertia $I = bh^3/12$ for a rectangular cross-section (b and h are the width and height of the cross-section, respectively). T is the axial extension, L and A are the length and cross-sectional area of the NW, respectively. Solving eqn (1) with the doubly clamped boundary condition gives a nonlinear *F–d* relation as[49] (EBT-A):

$$F = \frac{192EI}{L^3}f(k)d,\ f(k) = \frac{k}{48 - 192\tanh(\sqrt{k}/4)/\sqrt{k}} \quad (2)$$

here, k is solved from a complex transcendental equation,[49] with the asymptotic solution given as: $k = 6s(140 + s)/(350 + 3s)$, $s = d^2A/I$. By employing the whole elastic deformation region to fit with eqn (2), good agreement is found despite a discrepancy for the displacement below the nanowire thickness h (blue solid curve in Fig. 5 inset). The applicability of the theoretical model can be further assessed by firstly using the theoretical model to fit the experimental data at small displacement, and then examining the agreement between the experimental data and the extension of the fitting curve to include increasingly larger displacement. We thus use the data with the displacement less than half of the NW height to fit with eqn (2). It is found that although the nonlinearity of the *F–d* curve predicted by eqn (2) is in line with the experimental measurements, the force at larger deformation is overestimated, and the divergence increases with increasing displacement as shown in the blue dashed curve in Fig. 5 (pointed out as EBT-A), indicating the inaccuracy of the theoretical model.

There are several possible reasons for this discrepancy, such as approximations made while deriving the solution from the

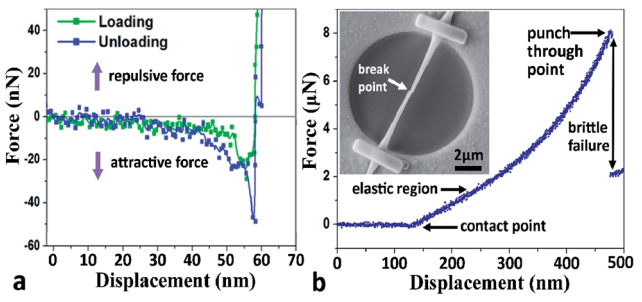

Fig. 4 (a) The attractive force between the AFM tip and the sample surface during loading and unloading processes. (b) *F–d* curve shows overall bending behavior of the $Na_2Ti_3O_7$ NW from experimental data; the inset SEM image shows the break point of the indentation.

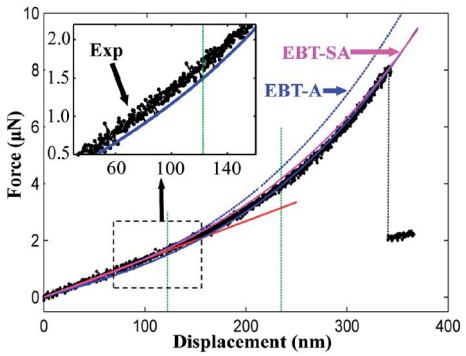

Fig. 5 *F–d* curve shows overall bending behavior of the $Na_2Ti_3O_7$ NW from experimental data (black curve). The blue solid line is the curve fitted using EBT-A model over the data from the whole elastic region; the inset shows the difference between the theory and experimental data at small displacements. The blue dash curve is the extension of the fitting curve of EBT-A using data at small displacement. The pink solid curve is the extension of the fitting curve of EBT-SA using data at small displacement considering the materials surface effects. The red line is the classical Euler–Bernoulli beam theory fitted to the experimental data in the linear *F–d* region.

governing equation, and measurement errors for the geometrical parameters of the NW, the force and the displacement. Another possible reason is that the model ignores the so-called surface effect, which is originated from the surface atoms who behave differently from their bulk counterparts (as they possess less neighbour atoms). In this regard, the NW is approximated as a "core–shell" structure, where the thin "shell" layer represents the surface atoms and possesses different mechanical properties from the "core" region. The detailed derivation of the modified beam model incorporated with surface effect (denoted as EBT-SA) can be found from the work reported by Zhan and Gu[50] and is summarised in ESI.† As shown in Fig. 5, although the impact from the surface effect is supposed to become significant while the cross-sectional size is much smaller than around 100 nm, the EBT-SA model is found to give an excellent prediction for the mechanical behaviour of the studied $Na_2Ti_3O_7$ NWs, whose wire width are around 400 nm. It can be concluded that the nonlinear elastic deformation of the $Na_2Ti_3O_7$ NW can be well explained by the beam model modified with axial extension effect, and the additional incorporation of the surface effect could further improve the theoretical prediction.

3.4. Mechanical properties

We then look into the mechanical properties of the $Na_2Ti_3O_7$ NW. To avoid the accumulating errors while using the modified beam models which contain several fitting parameters, the linear region (*i.e.*, small displacement) as indicated by the red line in Fig. 5, is adopted to interpret the mechanical properties of the NW. According to the beam theory, the influence from the axial extension can be ignored in this region, and the F and d for a doubly clamped beam follow a linear relation given by the classical Euler–Bernoulli beam model as:

$$F = \frac{192EI}{L^3}d \tag{3}$$

here the moment of inertia I is calculated by considering the NW as a continuum structure, and E is regarded as the overall or effective Young's modulus of the $Na_2Ti_3O_7$ NW.

Fig. 6 shows the estimated Young's moduli of $Na_2Ti_3O_7$ NWs with different lengths. To accurately determine the Young's modulus, NWs with similar diameters are repeated 5 to 10 times. No obvious trend is observed with the Young's modulus against the change of the $Na_2Ti_3O_7$ NW's length for wire width around 400 nm. The diversity in the Young's modulus might be slightly attributed to the defects/surface contamination of the single $Na_2Ti_3O_7$ NW. The variations of sizes between individual NWs can also lead to this diversity. More importantly, the $Na_2Ti_3O_7$ is monoclinic crystal, which possesses 13 independent elastic constants according to the generalized Hooke's law. In our experiments, although the crystal direction can be controlled along the length direction, the other two orthogonal lateral directions are uncertain which would lead to the variation of Young's modulus. The effective Young's modulus of the $Na_2Ti_3O_7$ NW ranges from 21.4 GPa to 45.5 GPa and the average value is estimated as 32.5 ± 7.4 GPa. It should be noted that there is currently no source on the Young's modulus of bulk sodium titanate materials.

Lastly, it is also of great interest to discuss the yielding strength of the $Na_2Ti_3O_7$ NW during bending. According to the

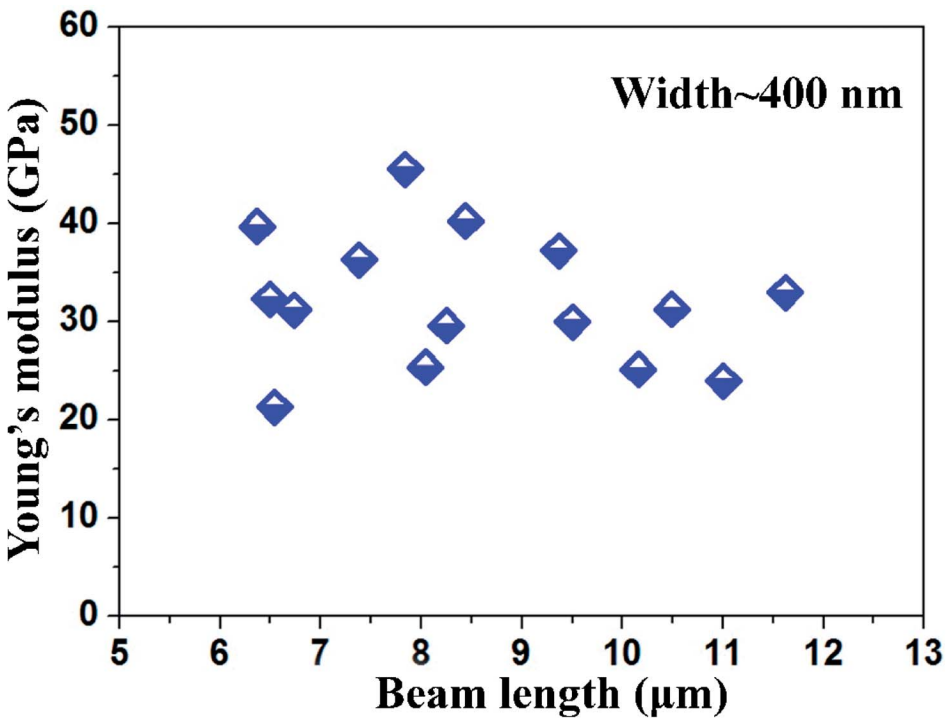

Fig. 6 Experimental results of effective Young's modulus of $Na_2Ti_3O_7$ NWs with different beam length.

Table 1 Summarized information on the parameters of the tested NWs and their yield strength

Sample	Width (nm)	Height (nm)	Length (nm)	F_{max} (nN)	σ_{max} (GPa)
1	274	256	4680	16 606	3.24
2	311	227	5030	14 730	3.46
3	442	322	8250	15 384	2.07
4	472	344	9520	15 703	2.00
5	488	356	10 160	22 242	2.74

classical mechanics, the top and bottom surfaces of the NW suffer the biggest stress. For a doubly clamped beam with a central loading, the maximum stress can be calculated according to the equation below[50]

$$\sigma_{max} = \frac{3F_{max}L}{4bh^2} \quad (4)$$

By using the maximum force in F–d curve before the onset of fracture, the yielding strength of various $Na_2Ti_3O_7$ NWs (length to width ratio around 20) are shown in Table 1 with the average yield strength as 2.7 ± 0.7 GPa. To compare with other NWs, the measured effective Young's modulus of $Na_2Ti_3O_7$ NW is in the same range with that reported for CdS (11–90 GPa)[51] and ZnS (35.9 ± 3.5 GPa)[52] for wire width between 200–400 nm. What is more, the measured yield strength of $Na_2Ti_3O_7$ NW has the same order with that of ZnO and GaN which are the most extensively characterized nanowires.[22]

4. Conclusion

In summary, we report the first study on the mechanical properties of $Na_2Ti_3O_7$ NWs through doubly-clamped bending experiments. It is found that the $Na_2Ti_3O_7$ NW exhibits a brittle behavior, and nonlinear elastic deformation is observed when the bending displacement is larger than half of the NW's height. With increasing displacement, the nonlinearity increases. Theoretical analysis reveals that the nonlinear elastic bending behavior of the $Na_2Ti_3O_7$ NW is attributed from the bending induced axial extension. The Young's modulus for the $Na_2Ti_3O_7$ NW is found to vary from 21.4 GPa to 45.5 GPa, with an average value of 32.5 ± 7.4 GPa. Yielding strength of the $Na_2Ti_3O_7$ NW is around 2.7 ± 0.7 GPa. The excellent mechanical properties presented by $Na_2Ti_3O_7$ NW suggest that they can be exceptionally useful as building blocks in the development of future nano-scale devices.

Acknowledgements

Supports from the ARC Discovery Project (DP130102120) and Central Analytical Research Facility (CARF) of Queensland University of Technology (QUT) are gratefully acknowledged.

References

1 D. Hennings, M. Klee and R. Waser, *Adv. Mater.*, 1991, **3**, 334–340.
2 R. E. Newnham, *MRS Bull.*, 1997, **22**, 20–34.
3 O. Rusina, O. Linnik, A. Eremenko and H. Kisch, *Chem.–Eur. J.*, 2003, **9**, 561–565.
4 J. J. Urban, W. S. Yun, Q. Gu and H. Park, *J. Am. Chem. Soc.*, 2002, **124**, 1186–1187.
5 D. Yu, J. Wu, L. Zhou, D. Xie and S. Wu, *Compos. Sci. Technol.*, 2000, **60**, 499–508.
6 T. Imai, Y. Nishida, M. Yamada, I. Shirayanagi and H. Matsubara, *J. Mater. Sci. Lett.*, 1987, **6**, 1257–1258.
7 H. Pan, X. Lu, X. Yu, Y. S. Hu, H. Li, X. Q. Yang and L. Chen, *Adv. Energy Mater.*, 2013, **3**, 1186–1194.
8 M. Shirpour, J. Cabana and M. Doeff, *Energy Environ. Sci.*, 2013, **6**, 2538–2547.
9 D. Yang, Z. Zheng, Y. Yuan, H. Liu, E. R. Waclawik, X. Ke, M. Xie and H. Zhu, *Phys. Chem. Chem. Phys.*, 2010, **12**, 1271–1277.
10 R. A. Aziz, I. I. Misnon, K. F. Chong, M. M. Yusoff and R. Jose, *Electrochim. Acta*, 2013, **113**, 141–148.
11 P. Hernández-Hipólito, M. García-Castillejos, E. Martínez-Klimova, N. Juárez-Flores, A. Gómez-Cortés and T. E. Klimova, *Catal. Today*, 2014, **220–222**, 4–11.
12 J. Q. Huang, Z. Huang, W. Guo, M. L. Wang, Y. G. Cao and M. C. Hong, *Cryst. Growth Des.*, 2008, **8**, 2444–2446.
13 D. Yang, S. Sarina, H. Zhu, H. Liu, Z. Zheng, M. Xie, S. V. Smith and S. Komarneni, *Angew. Chem., Int. Ed.*, 2011, **50**, 10594–10598.
14 H. Y. Zhu, Y. Lan, X. P. Gao, S. P. Ringer, Z. F. Zheng, D. Y. Song and J. C. Zhao, *J. Am. Chem. Soc.*, 2005, **127**, 6730–6736.
15 H. Liu, Z. Zheng, D. Yang, X. Ke, E. Jaatinen, J. C. Zhao and H. Y. Zhu, *ACS Nano*, 2010, **4**, 6219–6227.
16 H. Zhang, X. P. Gao, G. R. Li, T. Y. Yan and H. Y. Zhu, *Electrochim. Acta*, 2008, **53**, 7061–7068.
17 D. J. Yang, Z. F. Zheng, H. Y. Zhu, H. W. Liu and X. P. Gao, *Adv. Mater.*, 2008, **20**, 2777–2781.
18 F. Takahashi, Z. Sun, K. Fukushi, Y. Oshima and K. Yamamoto, *J. Supercrit. Fluids*, 2012, **61**, 126–133.
19 D. Hu, X. Kong, K. Mori, Y. Tanaka, K. Shinagawa and Q. Feng, *Inorg. Chem.*, 2013, **52**, 10542–10551.
20 T. Kennedy, E. Mullane, H. Geaney, M. Osiak, C. O'Dwyer and K. M. Ryan, *Nano Lett.*, 2014, **14**, 716–723.
21 S. Gong, W. Schwalb, Y. Wang, Y. Chen, Y. Tang, J. Si, B. Shirinzadeh and W. A. Cheng, *Nat. Commun.*, 2014, **5**, 1–8.
22 H. D. Espinosa, R. A. Bernal and M. A. Minary-Jolandan, *Adv. Mater.*, 2012, **24**, 4656–4675.
23 V. Pachauri, C. Subramaniam and T. Pradeep, *Chem. Phys. Lett.*, 2006, **423**, 240–246.
24 F. Cao, W. Hu, L. Zhou, W. Shi, S. Song, Y. Lei, S. Wang and H. Zhang, *Dalton Trans.*, 2009, **42**, 9246–9252.
25 T. Takahashi, K. Takei, E. Adabi, Z. Fan, A. M. Niknejad and A. Javey, *ACS Nano*, 2010, **4**, 5855–5860.

26 B. Wu, A. Heidelberg, J. J. Boland, J. E. Sader, X. M. Sun and Y. D. Li, *Nano Lett.*, 2006, **6**, 468–472.
27 B. Wu, A. Heidelberg and J. J. Boland, *Nat. Mater.*, 2005, **4**, 525–529.
28 B. Wen, J. E. Sader and J. J. Boland, *Phys. Rev. Lett.*, 2008, **101**, 1755021–1755024.
29 H. Zhang, J. Tang, L. Zhang, B. An and L. C. Qin, *Appl. Phys. Lett.*, 2008, **92**, 1731211–1731213.
30 X. Li, H. Gao, C. J. Murphy and K. K. Caswell, *Nano Lett.*, 2003, **3**, 1495–1498.
31 S. Cuenot, S. Demoustier-Champagne and B. Nysten, *Phys. Rev. Lett.*, 2000, **85**, 1690–1693.
32 J. P. Salvetat, G. A. D. Briggs, J. M. Bonard, R. R. Bacsa, A. J. Kulik, T. Stöckli, N. A. Burnham and L. Forró, *Phys. Rev. Lett.*, 1999, **82**, 944–947.
33 A. Kis, S. Kasas, B. Babić, A. J. Kulik, W. Benoit, G. A. D. Briggs, C. Schönenberger, S. Catsicas and L. Forro, *Phys. Rev. Lett.*, 2002, **89**, 2481011–2481014.
34 G. Y. Jing, H. L. Duan, X. M. Sun, Z. S. Zhang, J. Xu, Y. D. Li, J. X. Wang and D. P. Yu, *Phys. Rev. B: Condens. Matter Mater. Phys.*, 2006, **73**, 2354091–2354096.
35 Y. Chen, B. L. Dorgan, D. N. McIlroy and A. D. Eric, *J. Appl. Phys.*, 2006, **100**, 1043011–1043017.
36 Y. Chen, I. Stevenson, R. Pouy, L. Wang, D. N. McIlroy, T. Pounds, M. G. Norton and D. E. Aston, *Nanotechnology*, 2007, **18**, 1357081–1357088.
37 D. A. Walters, L. M. Ericson, M. J. Casavant, J. Liu, D. T. Colbert, K. A. Smith and R. E. Smalley, *Appl. Phys. Lett.*, 1999, **74**, 3803–3805.
38 I. W. Frank, D. M. Tanenbaum, A. M. Van der Zande and P. L. McEuen, *J. Vac. Sci. Technol., B: Nanotechnol. Microelectron.: Mater., Process., Meas., Phenom.*, 2007, **25**, 2558–2561.
39 B. Lee and R. E. Rudd, *Phys. Rev. B: Condens. Matter Mater. Phys.*, 2007, **75**, 1953281–1953315.
40 H. Zhan and Y. Gu, *Comput. Mater. Sci.*, 2012, **55**, 73–80.
41 H. Zhan and Y. Gu, *J. Phys. D: Appl. Phys.*, 2012, **45**, 4653041–4653110.
42 H. F. Zhan, Y. T. Gu, C. Yan, X. Q. Feng and P. K. D. V. Yarlagadda, *Comput. Mater. Sci.*, 2011, **50**, 3425–3430.
43 S. Andersson and A. Wadsley, *Acta Crystallogr.*, 1962, **15**, 194–201.
44 Q. Chen, G. H. Du, S. Zhang and L. M. Peng, *Acta Crystallogr., Sect. B: Struct. Sci.*, 2002, **58**, 587–593.
45 S. Andersson and A. Wadsley, *Acta Crystallogr.*, 1961, **14**, 1245–1249.
46 O. Yakubovich and V. Kireev, *Crystallogr. Rep.*, 2003, **48**, 24–28.
47 B. Cappella and G. Dietler, *Surf. Sci. Rep.*, 1999, **34**, 1–104.
48 H. J. Butt, B. Cappella and M. Kappl, *Surf. Sci. Rep.*, 2005, **59**, 1–152.
49 A. Heidelberg, L. T. Ngo, B. Wu, M. A. Phillips, S. Sharma, T. I. Kamins, J. E. Sader and J. J. Boland, *Nano Lett.*, 2006, **6**, 1101–1106.
50 H. Zhan and Y. Gu, *J. Appl. Phys.*, 2012, **111**, 0843051–0843059.
51 P. Gao, K. Liu, L. Liu, Z. Wang, Z. Liao, Z. Xu, W. Wang, X. Bai, E. Wang and Y. Li, *J. Electron Microsc.*, 2010, **59**, 285–289.
52 X. Li, X. Wang, Q. Xiong and P. C. Eklund, *Nano Lett.*, 2005, **5**, 1982–1986.
53 J. E. Sader, J. W. Chon and P. Mulvaney, *Rev. Sci. Instrum.*, 1999, **70**, 3967–3969.